

PAPER

Efficient small molecule bulk heterojunction solar cells with high fill factors *via* introduction of π -stacking moieties as end group†

Cite this: *J. Mater. Chem. A*, 2013, **1**, 1801

Guangrui He,^a Zhi Li,^a Xiangjian Wan,^a Jiaoyan Zhou,^a Guankui Long,^a Shuzhong Zhang,^b Mingtao Zhang^c and Yongsheng Chen^{*a}

Three new oligothiophene derivatives with an acceptor–donor–acceptor structure incorporating 1,3-indanedione or the derivative of 1,3-indanedione units as the terminal acceptor groups—DIN7T, DINCN7T and DDIN7T—have been designed and synthesized for solution-processable small molecule BHJ solar cells. The impacts of these different end dye moieties on the optical absorption, solubility, electrochemical properties, morphology, mobility and solar cell performance were studied. All three compounds exhibit broad and highly efficient solar absorption with a low bandgap. The DIN7T-based BHJ solar cell device achieved a PCE of 4.93% and a high fill factor of 0.72, under illumination of AM 1.5, 100 mW cm⁻².

Received 29th September 2012
Accepted 28th November 2012

DOI: 10.1039/c2ta00496h

www.rsc.org/MaterialsA

Introduction

In recent years, polymer solar cells (PSCs) comprised of a bulk heterojunction (BHJ) layer have attracted significant attention due to their ease of synthesis, potential to enable low-cost manufacturing and capability to fabricate flexible large-area devices.^{1–5} Power conversion efficiencies (PCEs) above 9% have been achieved⁶ due to significant improvements in active material design,^{7–9} device structure and fabricating techniques,^{10–14} morphology control and characterization methods,^{15,16} *etc.*^{17,18}

In contrast to PSCs, solution-processed small molecule BHJ (SM BHJ) solar cells, combining the advantages of high purity, well-defined structure and molecular weight without batch-to-batch variation,^{19–23} have stimulated more and more attention.^{24–29} Recently, significant progress has been made and PCEs of 6–7% have been achieved for SM BHJs.^{30–33} In order to take full advantage of the properties of small molecules, more efficient and systemic efforts are highly desired. Currently, the

active materials, especially the donor materials are still the first key factor for high PCE SM BHJ solar cells.

Previously, we have reported a series of molecules using oligothiophene as the backbone with different end groups.^{30,34–36} In these molecules, DCAO7T³⁵ and DERHD7T³⁰ based devices gave efficiencies of about 5 and 6%, respectively, with PC₆₁BM as the electron acceptor. These high efficiencies warrant expansion of the work towards exploring new electron deficient groups. Recently, we described two similar analogues, DTDMP7T and D2R(8 + 2)7T.³⁶ These two molecules have broad and efficient absorption, but the performances of solar cells based on them were not as good as those based on DERHD7T and DCAO7T due to the poor stacking of the molecules in the solid state. It has been found that the terminal electron units have a great influence on the absorption, energy levels, mobilities and final solar cell performances of the corresponding molecules.

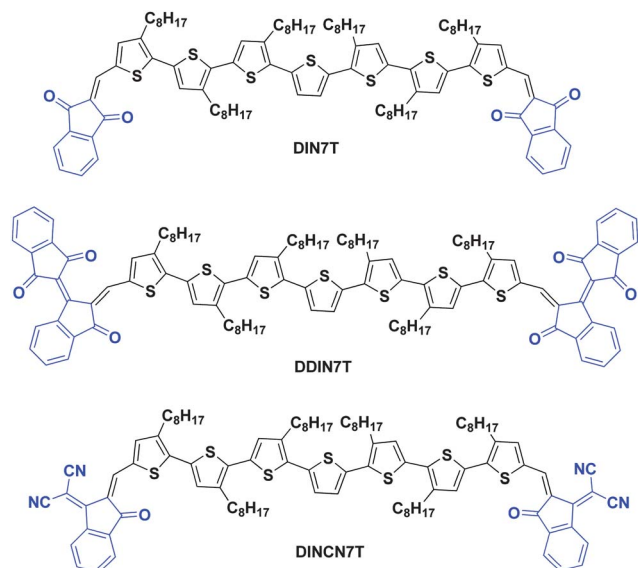
Replacing the central thiophene unit of oligothiophene with a better planar structure such as the dithienosilole unit³⁷ or the benzo[1,2-*b*:4,5-*b'*]dithiophene (BDT) unit³⁸ has proven to efficiently improve the packing situation of donors and the SM BHJs performance, especially the FF, in our recent work. Fréchet and coworkers reported that introduction of π -stacking moieties onto the ends of small molecules can facilitate favorable π - π interactions in the film, leading to enhanced charge transport between adjacent molecules.³⁹ Thus, we postulated that the end groups of the A–D–A type molecules can also serve as π -stacking regulators, supplying an easier route to adjust the aggregation of A–D–A dyes. With this strategy in mind, we have designed and synthesized three molecules with three dye end units (Scheme 1), 1,3-indanedione (IN), 2-(3-oxo-2,3-dihydroinden-1-ylidene)malononitrile

^aKey Laboratory for Functional Polymer Materials and Centre for Nanoscale Science and Technology, Institute of Polymer Chemistry, College of Chemistry Nankai University, Tianjin 300071, China. E-mail: yschen99@nankai.edu.cn; xjwan@nankai.edu.cn; Fax: +86-(22)-2349-9992

^bState Key Laboratory of Elemento-Organic Chemistry, Nankai University, Tianjin 300071, China. E-mail: zhangsz@nankai.edu.cn

^cComputational Center for Molecular Science, Nankai University, Tianjin 300071, China. E-mail: zhangmt@nankai.edu.cn

† Electronic supplementary information (ESI) available: Spectra of ¹H NMR, ¹³C NMR and HRMS of these three new molecules. Experimental details of SM BHJs test, solubility, calculated molecular structure and mobility curves, *etc.* See DOI: 10.1039/c2ta00496h



Scheme 1 The chemical structures of DIN7T, DDIN7T and DINC7T.

(INCN) and [1,2']biindenylidene-3,1',3'-trione (DIN), as the end acceptor moieties. These acceptor units, with high electron affinities, have been reported to be chromophores with strong optical absorptions and good planar structures.⁴⁰ As expected, these materials indeed show broad and efficient sunlight harvesting and good stacking in the film, except for DDIN7T, which has a twisted molecular architecture. SM BHJ devices were fabricated using these compounds as the donor and PC₆₁BM, PC₇₁BM and indene C₆₀ bisadduct (ICBA) as the acceptors. A PCE of 4.93% was achieved with an open circuit voltage (V_{oc}) of 0.80 V, a short circuit current density (J_{sc}) of 8.54 mA cm⁻² and a FF of 0.72 for DIN7T. In contrast, DDIN7T-based SM BHJs display a much lower PCE of 0.66% with a V_{oc} of 0.76 V, J_{sc} of 3.12 mA cm⁻² and FF of 0.27. The unexpectedly low solubility of DINC7T prevents its application in SM BHJs.

Experimental

Materials

All reactions and manipulations were carried out under argon atmosphere with the use of standard Schlenk techniques. All starting materials, unless otherwise specified, were purchased from commercial suppliers and used without further purification. Diformylsepthiophene (DF7T) (5,5''''-diformyl-3,3',3'',3''',3''''-sextioctyl-2,5':2'',5''':2'',2''':5'''';5''''':5'''''';5''''''':2''''''''-septhiophene),⁴¹ 2-(3-oxo-2,3-dihydroinden-1-ylidene)-malononitrile (INCN) and [1,2']biindenylidene-3,1',3'-trione (DIN) were prepared according to the literature.⁴⁰

Nuclear magnetic resonance (NMR) spectra were taken on a Bruker AV400 Spectrometer. MALDI-TOF spectra were performed on a Bruker Autoflex III instrument. Thermogravimetric analysis (TGA) was carried out on a NETZSCH STA 409PC instrument under nitrogen gas flow with a 10 °C min⁻¹ heating rate. UV-Vis spectra were obtained with a JASCO V-570 spectrophotometer. The organic molecule films on quartz used for

absorption spectral measurement were prepared by spin-coating their chloroform solutions. X-Ray diffraction (XRD) experiments were performed on a Rigaku D/max-2500 X-ray diffractometer with Cu-K α radiation ($k = 1.5406 \text{ \AA}$) at a generator voltage of 40 kV and a current of 100 mA. Cyclic voltammetry (CV) experiments were performed with a LK98B II Microcomputer-based Electrochemical Analyzer in CH₂Cl₂ solutions. All measurements were carried out at room temperature with a conventional three-electrode configuration employing a glassy carbon electrode as the working electrode, a saturated calomel electrode (SCE) as the reference electrode, and a Pt wire as the counter electrode. Dichloromethane was distilled from calcium hydride under dry nitrogen immediately prior to use. Tetrabutylammonium phosphorus hexafluoride (Bu₄NPF₆, 0.1 M) in dichloromethane was used as the supporting electrolyte, and the scan rate was 100 mV s⁻¹.

Hole mobility was measured according to a similar method described in the literature,^{42,43} using a diode configuration of ITO/PEDOT:PSS/DIN7T or DDIN7T/Al by taking dark current in the range of 0–8 V and fitting the results to a space charge limited form, where the SCLC is described by $J = 9\epsilon_0\epsilon_r\mu_h V^2/8L^3$ where J is the current density, L is the film thickness of the active layer, μ_h is the hole mobility, ϵ_r is the relative dielectric constant of the transport medium, ϵ_0 is the permittivity of free space ($8.85 \times 10^{-12} \text{ F m}^{-1}$), and V , the internal voltage, is defined as $V = V_{app} - V_r - V_{bi}$, where V_{app} is the applied voltage to the device, V_r is the voltage drop due to contact resistance and series resistance across the electrodes, and V_{bi} is the built-in voltage due to the relative work function difference of the two electrodes.

The photovoltaic devices were fabricated with a structure of glass/ITO/PEDOT:PSS/donor:acceptor/LiF or Ca/Al. The ITO-coated glass substrates were cleaned by ultrasonic treatment in detergent, deionized water, acetone, and isopropyl alcohol under ultrasonication for 15 min each and subsequently dried by a nitrogen flow. A thin layer of PEDOT:PSS (Baytron P VP Al 4083, filtered at 0.45 μm) was spin-coated (3000 rpm, *ca.* 40 nm thick) onto the ITO surface. After being baked at 150 °C for 20 min, the substrates were transferred into an argon-filled glove box. Subsequently, the active layer was spin-casted from different blend ratios (w/w) of donor (8 mg mL⁻¹) and PC₆₁BM in chloroform solution at 1500 rpm for 20 s on the ITO/PEDOT:PSS substrate without further special treatments. The active layer thickness was measured using a Dektak 150 profilometer. Finally, ~ 1 nm LiF or 20 nm Ca layer and 80 nm Al layer were deposited on the active layer under high vacuum ($< 3 \times 10^{-4}$ Pa). The effective area of each cell was $\sim 4 \text{ mm}^2$ defined by masks for all the solar cell devices discussed in this work.

The transmission electron microscopy (TEM) investigation was performed on a JEOL JEM2010FIF operated at 200 kV. Atomic force microscopy (AFM) investigation was performed using a Bruker MultiMode 8 in “tapping” mode. The current density–voltage (J – V) curves of photovoltaic devices were obtained by a Keithley 2400 source-measure unit. The photocurrent was measured under simulated 100 mW cm⁻² AM 1.5G irradiation using a xenon lamp-based solar simulator [Oriol

96000 (AM 1.5G)] in an argon-filled glove box. Simulator irradiance was calibrated using a certified silicon diode. External quantum efficiency (EQE) values of the encapsulated devices were measured using a lock-in amplifier (SR810, Stanford Research Systems). The devices were illuminated by monochromatic light from a 150 W xenon lamp passing through an optical chopper and a monochromator. Photon flux was determined by a calibrated standard silicon photodiode.

Synthesis

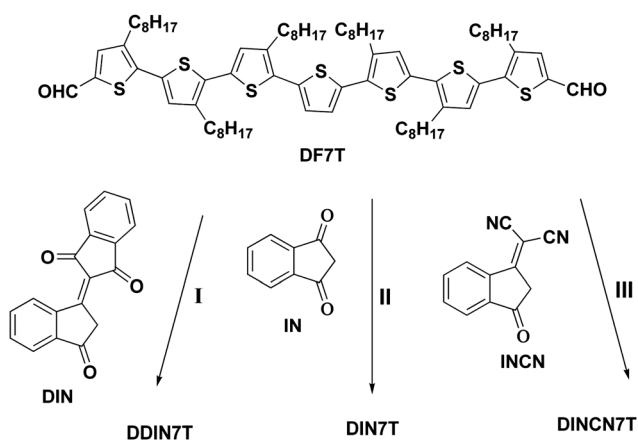
The synthesis routes to DIN7T, DDIN7T and DINCN7T are shown in Scheme 2.

DIN7T. Diformylseptithiophene (DF7T) (130 mg, 0.10 mmol) was dissolved in a solution of dry CHCl_3 (50 mL). Then 1,3-indanedione (IN) (146 mg, 1.00 mmol) and three drops of triethylamine were added and the resulting solution was stirred for 20 h, under argon, at room temperature. After removal of solvent, the crude product was dissolved in 8 mL of chloroform, then precipitated from methanol and the precipitate was filtered off. This procedure was repeated several times to absolutely remove 1,3-indanedione. Then, the product was separated by chromatography using silica gel and a mixture of dichloromethane and petroleum ether (1 : 1) as eluent to afford DIN7T as a black solid (120 mg, 77% yield). ^1H NMR (400 MHz, CDCl_3): δ 7.94 (m, 4H), 7.85 (s, 2H), 7.75 (m, 6H), 7.29 (s, 2H), 7.12 (s, 2H), 7.04 (s, 2H), 2.82 (m, 12H), 1.72 (m, 12H), 1.45 (m, 12H), 1.25–1.41 (m, 48H), 0.89 (m, 18H). ^{13}C NMR (400 MHz, CDCl_3): δ 190.391, 189.755, 145.535, 145.192, 142.003, 140.675, 140.493, 140.434, 140.162, 135.688, 134.902, 134.686, 134.395, 133.509, 133.374, 132.842, 131.091, 130.852, 129.098, 126.101, 123.565, 122.889, 122.705, 31.931, 31.895, 30.627, 30.544, 30.044, 29.678, 29.577, 29.516, 29.444, 29.384, 29.342, 29.307, 22.708, 14.139. HRMS (MALDI-FTMS) m/z : calcd for $\text{C}_{96}\text{H}_{120}\text{O}_4\text{S}_7$ $[\text{M}]^+$, 1561.7265; found, 1561.7316.

DINCN7T. Diformylseptithiophene (DF7T) (130 mg, 0.10 mmol) was dissolved in a solution of dry CHCl_3 (50 mL). Then 2-

(3-oxo-2,3-dihydroinden-1-ylidene)malononitrile (INCN) (194 mg, 1.00 mmol) and 0.3 mL of pyridine were added and the resulting solution was stirred for 20 h under argon, at room temperature. The resulting mixture was poured into methanol and the precipitate was filtered off. The crude product was dissolved in 20 mL of hot chloroform, then precipitated from methanol and the precipitate was filtered off. This procedure was repeated several times to absolutely remove any remaining reactants. Then, the product was separated by chromatography using silica gel and a mixture of dichloromethane and petroleum ether (3 : 2) as eluent to afford DINCN7T as a black solid (130 mg, 78% yield). The molecule was recrystallized twice using CHCl_3 and ethyl acetate. ^1H NMR (400 MHz, CDCl_3): δ 8.813 (s, 2H), 8.703 (d, $J = 6.8$, 2H), 7.942 (d, $J = 6.8$, 2H), 7.763 (m, 4H), 7.667 (s, 2H), 7.386 (s, 2H), 7.145 (s, 2H), 7.074 (s, 2H), 2.846 (m, 12H), 1.727 (m, 12H), 1.447 (m, 12H), 1.225–1.406 (m, 48H), 0.888 (m, 18H). HRMS (MALDI-FTMS) m/z : calcd for $\text{C}_{102}\text{H}_{120}\text{N}_4\text{O}_2\text{S}_7$ $[\text{M}]^+$, 1657.7490; found, 1657.7544.

DDIN7T. Diformylseptithiophene (DF7T) (130 mg, 0.10 mmol) was dissolved in a solution of dry CH_2Cl_2 (50 mL) and 0.3 mL of butylamine was added. The resulting solution was stirred in the dark at room temperature and was monitored by TLC. When the reaction was finished, the solvent was removed *in vacuo* and the resultant solid was dissolved in 20 mL of chloroform. Then, [1,2']-biindenylidene-3,1',3'-trione (DIN) (137 mg, 0.5 mmol) and 10 mL of acetic anhydride were added and the resulting solution was refluxed overnight. The resulting mixture was poured into methanol and the precipitate was filtered off. The crude product was dissolved in 20 mL of chloroform, then precipitated from methanol and the precipitate was filtered off. This procedure was repeated several times to absolutely remove any remaining reactants. Then, the product was separated by chromatography using silica gel and a mixture of dichloromethane and petroleum ether (3 : 2) as eluent to afford DDIN7T as a black solid (110 mg, 60% yield). The molecule was recrystallized twice using CHCl_3 and ethyl acetate. ^1H NMR (400 MHz, CDCl_3): δ 8.951 (d, $J = 6.8$, 2H), 8.391 (s, 2H), 7.962 (m, 4H), 7.878 (d, $J = 6.8$, 2H), 7.770 (m, 4H), 7.659 (m, 6H), 7.360 (s, 2H), 7.130 (s, 2H), 7.052 (s, 2H), 2.828 (m, 12H), 1.727 (m, 12H), 1.448 (m, 12H), 1.220–1.410 (m, 48H), 0.886 (m, 18H). ^{13}C NMR (400 MHz, CDCl_3): δ 190.557, 190.355, 189.198, 161.497, 146.929, 143.305, 143.252, 141.625, 140.795, 140.373, 138.327, 134.650, 134.538, 134.374, 133.686, 133.272, 131.105, 130.307, 129.027, 124.518, 122.900, 122.658, 31.951, 31.911, 29.723, 29.545, 29.485, 29.455, 29.368, 29.313, 22.720, 14.137. HRMS (MALDI-FTMS) m/z : calcd for $\text{C}_{90}\text{H}_{124}\text{N}_4\text{O}_6\text{S}_7 + \text{Na}$ $[\text{M} + \text{Na}]^+$, 1840.7667; found, 1840.7677.



Scheme 2 Synthesis routes to the compounds: (I) (1) butylamine, CH_2Cl_2 ; (2) DIN, CHCl_3 , acetic anhydride, Ar, reflux, overnight; (II) CHCl_3 , triethylamine, Ar, room temperature; (III) CHCl_3 , pyridine, Ar, room temperature.

Results and discussion

Synthesis and thermal stability of the compounds

DIN7T, DINCN7T and DDIN7T were synthesized by the routes shown in Scheme 2. DIN7T and DINCN7T were obtained *via* Knoevenagel reaction by directly treating their corresponding acceptor unit precursors, IN and INCN, with the aldehyde-bearing precursor DF7T in the presence of triethylamine or pyridine. DDIN7T was synthesized by a two-step process. Firstly,

the aldehyde-bearing precursor DF7T was activated by butylamine to afford the aldimine. Then, the target molecule DDIN7T was obtained by treating the aldimine with the excess amount of DIN, in the solution of chloroform and acetic anhydride.

Thermogravimetric analysis (TGA) suggests that DIN7T, DINCN7T and DDIN7T exhibit good stability with a decomposition temperature (T_d) greater than 300 °C under N_2 atmosphere (see Fig. 1).

Solubility and optical absorption

The solubilities of these three new molecules, together with several related molecules we reported before, were determined in $CHCl_3$ at room temperature.⁴⁴ As listed in Table 1, we can see that the acceptor unit of the molecules has a large impact on the solubility. As expected, DCAO7T has the largest solubility in $CHCl_3$ (204 $mg\ mL^{-1}$). The solubility decreases from DERHD7T (104 $mg\ mL^{-1}$) to DTDMP7T (32 $mg\ mL^{-1}$) and D2R(8 + 2)7T (29 $mg\ mL^{-1}$). The solubility of the new molecule DIN7T in $CHCl_3$ is up to 40 $mg\ mL^{-1}$, larger than that of DTDMP7T and D2R(8 + 2)7T. Replacing the IN with DIN reduces the solubility to 17 $mg\ mL^{-1}$. However, surprisingly, the similar acceptor unit INCN reduces the solubility substantially to 4.6 $mg\ mL^{-1}$.

The UV-vis absorption spectra of DIN7T, DINCN7T and DDIN7T in diluted chloroform solution ($10^{-5}\ mol\ L^{-1}$) and at solid films prepared by spin coating are shown in Fig. 2. The important optical absorption data of these three new molecules, together with those of DCAO7T and DERHD7T for comparison, are summarized in Table 1.

Compared with the absorption peaks at 492 nm of DCAO7T solution and 508 nm of DERHD7T solution, DIN7T (541 nm), DINCN7T (618 nm) and DDIN7T (645 nm) have a large red-shift of about 40–140 nm (Fig. 2a). In addition, the absorption coefficients of DIN7T (50 $L\ g^{-1}\ cm^{-1}$) and DINCN7T (51 $L\ g^{-1}\ cm^{-1}$) in $CHCl_3$ are comparable to that of DERHD7T (56 $L\ g^{-1}\ cm^{-1}$), while DDIN7T has a slightly lower absorption coefficient (38 $L\ g^{-1}\ cm^{-1}$).

Additionally, as shown in Fig. 2b, DIN7T film, which shows a broader absorption from 350 to 900 nm, displays a red-shifted λ_{max} at 630 nm with a strong vibronic shoulder at 692 nm. DINCN7T has a red-shifted absorption peak at 718 nm with a

broader absorption from 400 to 950 nm and also a vibronic shoulder at 802 nm. DDIN7T film has an absorption peak at 684 nm, without a vibronic shoulder peak. The optical band gaps of DIN7T, DINCN7T and DDIN7T thin films were estimated from the onset of the film absorption spectra to be 1.49, 1.33 and 1.20 eV (Table 1), lower than those of the compared compounds DCAO7T and DERHD7T.

Compared with the solution absorption, DIN7T and DINCN7T films have vibronic shoulder peaks and are largely red-shifted about 100 nm, similar to DCAO7T and DERHD7T. In contrast, DDIN7T film has a much smaller red-shifted peak without a vibronic shoulder. This means that DIN7T and DINCN7T have the same efficient packing as DCAO7T and DERHD7T, much better than that of DDIN7T.

Electrochemical properties and electronic energy levels

The electrochemical properties of DIN7T, DINCN7T and DDIN7T were investigated by cyclic voltammetry (CV). The potentials were internally calibrated using the ferrocene/ferrocenium of the (Fc/Fc⁺) redox couple (4.8 eV below the vacuum level). As shown in Fig. 3, the energy levels of the HOMO and LUMO, which are -4.97 and -3.44 eV for DIN7T, -5.02 and -3.72 eV for DINCN7T, and -4.90 and -3.86 eV for DDIN7T, respectively, were calculated from the onset oxidation and reduction potential. The electrochemical band gaps of DIN7T, DINCN7T and DDIN7T are estimated to be 1.53, 1.30 and 1.04 eV, respectively. The values of the bandgaps, HOMO and LUMO energy levels of the two compounds, along with those of DCAO7T, DERHD7T and other molecules for comparison, are listed in Table 1. From Table 1, we can see that the HOMO energy levels of these molecules are very similar (-5.0 to -5.1 eV), which is predominantly determined by the donor moiety (oligothiophene unit). In contrast to the HOMOs, the LUMO energy levels of these molecules changed distinctly, leading to different bandgaps of these molecules, from 1.84 to 1.04 eV. These results are consistent with the optical data and demonstrate that the band gaps of these molecules can be tuned effectively through introducing different acceptor terminal units. The slight differences in the bandgap values determined from CV and optical methods could arise from many factors, including error from onset point selection in the UV spectra, the electrode and the solvent in the CV test, *etc.*^{45,46}

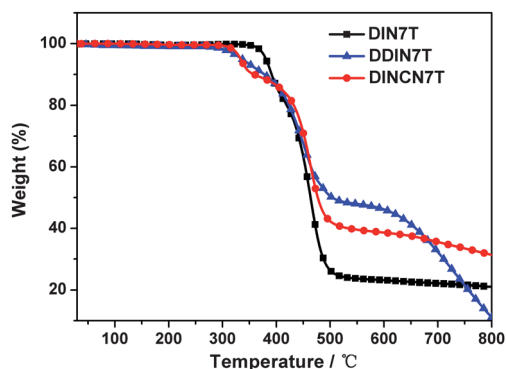


Fig. 1 TGA plot of DIN7T, DINCN7T and DDIN7T.

X-Ray diffraction (XRD) and structure calculation

The structural orders of pristine DIN7T, DINCN7T and DDIN7T were investigated by X-ray diffraction (XRD) analysis, for the films of DIN7T and DDIN7T spin-coated from $CHCl_3$ solutions onto glass substrates and the films of DINCN7T dropped onto glass substrate. The XRD patterns of DIN7T, DINCN7T and DDIN7T films, together with those of DCAO7T and DERHD7T, are shown in Fig. 4.

The pristine DIN7T film exhibited a strong first-order diffraction peak (100) at $2\theta = 4.6^\circ$, corresponding to a d_{100} spacing value of 19.3 Å for the distance between the planes of the main conjugation chains of these molecules. The diffraction

Table 1 Optical and electrochemical data of DCAO7T, DERHD7T, DIN7T and previously reported compounds

Compounds	λ_{\max} solution (nm)	ϵ solution ($L g^{-1} cm^{-1}$)	λ_{\max} film (nm)	(E_g^{opt}) film (eV)	E_g^{cv} (eV)	HOMO (eV)	LUMO (eV)	Solubility ($mg mL^{-1}$)
D2R(8 + 2)7T ^a	534	44	584	1.70	1.70	-5.09	-3.39	32
DTDMP7T ^a	537	35	605	1.67	1.62	-5.12	-3.50	29
DCAO7T ^b	492	34	580	1.74	1.84	-5.13	-3.29	204
DERHD7T ^c	508	56	618	1.69	1.72	-5.00	-3.28	104
DIN7T	541	50	630, 692	1.49	1.53	-4.97	-3.44	40
DINC7T	618	51	718, 802	1.33	1.30	-5.02	-3.72	4.6
DDIN7T	645	38	684	1.20	1.04	-4.90	-3.86	17

^a Data from ref. 36. Solubility data of all seven compounds were tested in this work. ^b Data from ref. 35. ^c Data from ref. 30.

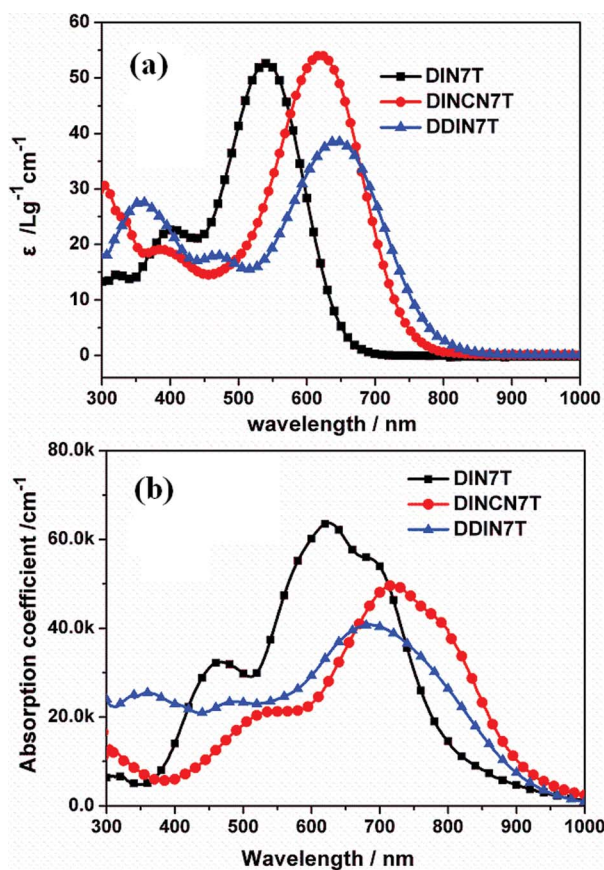


Fig. 2 (a) Absorption spectra of DIN7T, DINC7T and DDIN7T in chloroform solution; (b) absorption spectra of DIN7T, DINC7T and DDIN7T as films.

peaks at $2\theta = 9.2$ and 13.6° corresponding to d -spacings of 9.7 and 6.5 Å for second and third order are also observed. For DINC7T, the (100) and (200) diffraction peaks can be seen. The diffraction result of DIN7T and DINC7T indicated that highly organized assembly and crystallinity of these π -conjugated molecules were formed in the solid state, which could be explained by the planar structure, supported by the density functional theory (DFT) calculation result obtained from the Gaussian 09 model⁴⁷(see Fig. S3 and S4[†]). In contrast, no clear diffraction peak was observed for DDIN7T, meaning a poor stacking of DDIN7T in the film, for the molecule has a twisted

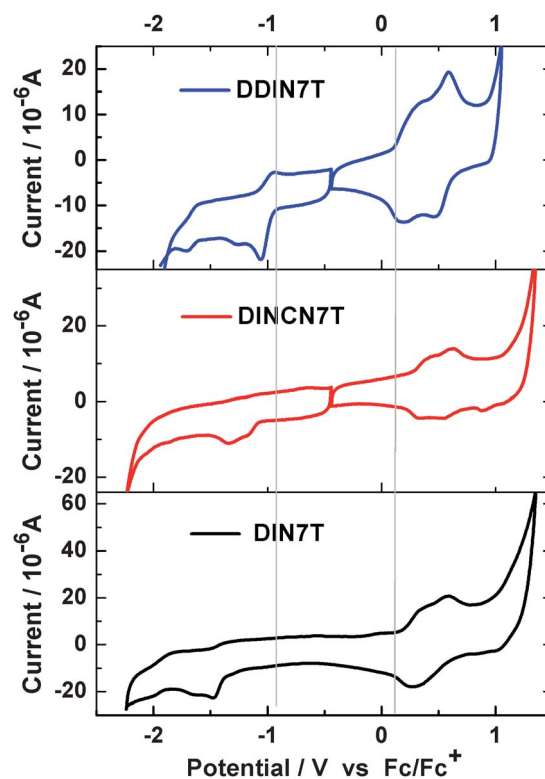


Fig. 3 Cyclic voltammograms of DIN7T, DINC7T and DDIN7T in a dichloro-methane solution of 0.1 mol L⁻¹ Bu₄NPF₆ with a scan rate of 100 mV s⁻¹ on a Pd/C electrode.

molecular architecture (Fig. S5[†]). Furthermore, the XRD of the blended films of these three molecules with PC₆₁BM have similar patterns with their pristine XRD (Fig. S7[†]).

To give a rough estimate of the crystallinity of the new molecule DIN7T compared with that of DERHD7T and DCAO7T, we chose the diffraction peak corresponding to the (100) orientation of the organic crystallite to study.^{8,48,49} It is important to note that the films of DIN7T, DERHD7T and DCAO7T have similar thicknesses and were prepared *via* the same procedure. From Fig. 4, it can be seen that the intensity of the diffraction peak increased substantially from DERHD7T and DCAO7T to DIN7T, which is consistent with the strategy that using a better planar terminal group can increase overall

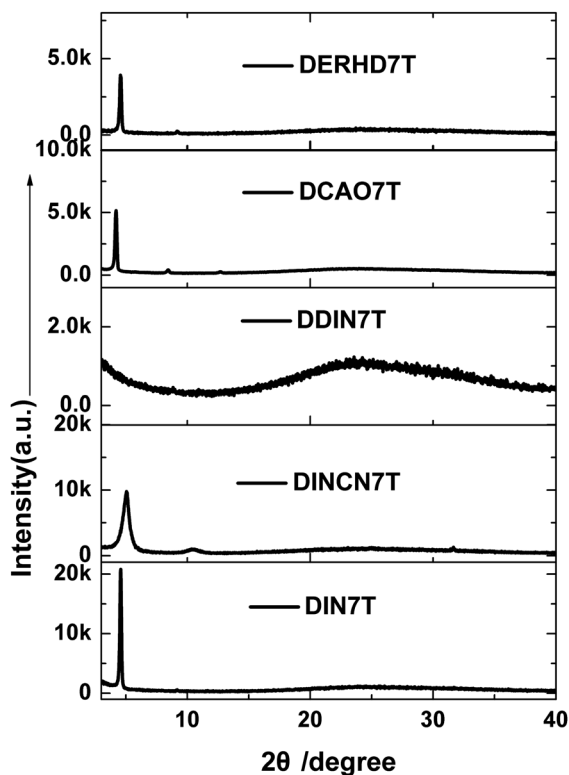


Fig. 4 XRD patterns of DCAO7T, DERHD7T, DDIN7T and DIN7T films spin-coated from CHCl_3 onto glass substrate. DINC7T film was dropped onto glass substrate.

planarity and crystallinity of the molecule in the film. Moreover, the full width at half-maximum (FWHM)²¹ result shown in Fig. 4 and Table S3† also confirmed the above conclusion.

Hole mobility

The hole mobility of the pristine DIN7T and DDIN7T films was measured by the space charge limited current (SCLC) method. As plotted in Fig. S16 and S17† and listed in Table 2, the hole mobility value of DIN7T film is $1.73 \times 10^{-4} \text{ cm}^2 \text{ V}^{-1} \text{ s}^{-1}$, similar to DCAO7T and DERHD7T from our previous work. DDIN7T film shows a much smaller hole mobility of $3.0 \times 10^{-5} \text{ cm}^2 \text{ V}^{-1} \text{ s}^{-1}$. These hole mobility results can be explained by the XRD data above.

Photovoltaic performance

Bulk-heterojunction organic solar cells were fabricated by using the two new organic molecules DIN7T and DDIN7T as the donor materials, and PC_{61}BM as the acceptor material, using the conventional solution spin-coating process. The device structure is ITO/PEDOT:PSS/photoactive layer/LiF or Ca/Al. Device optimizations were conducted by varying the weight ratios of donor vs. acceptor (summarized in Tables S3 and S4† and shown in Fig. S8–S15†). The optimal typical current density–voltage (J – V) curves of the SM BHJs are shown in Fig. 5 and the optimal results are summarized in Table 2. For DINC7T, its poor solubility prevents its application in SM BHJ devices *via* spin coating.

For DDIN7T, the optimal efficiency was obtained from the device with the active layer comprised of a blend of DDIN7T and PC_{61}BM with a weight ratio of 1 : 1 and an optimized thickness of about 90 nm, using Ca/Al as the cathode. This SM BHJ device gave a V_{oc} of 0.76 V, a J_{sc} of 3.14 mA cm^{-2} , a fill factor (FF) of 0.28 and a PCE of 0.66%. Compared to our previously reported molecules, DCAO7T, DERHD7T, DTDMP7T and D2R(8 + 2)7T, the lower open circuit voltage of DDIN7T may be due to its high HOMO. Furthermore, the LUMO difference between DDIN7T and PC_{61}BM is significantly lower than that of the other molecules, which means a lower driving force for forward electron transfer between the donor and acceptor, together with poor

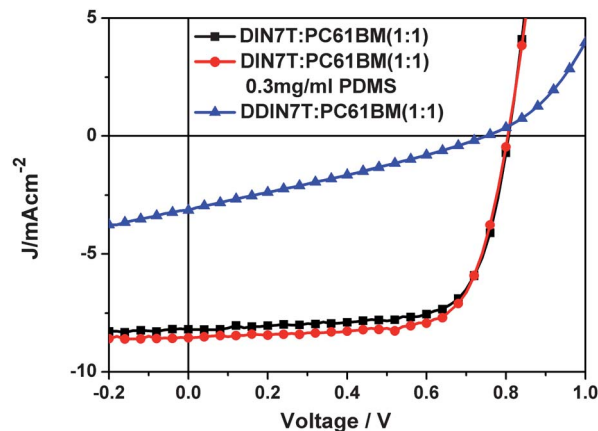


Fig. 5 Current density–voltage characteristics of the optimized SM BHJ devices based on the blend of DIN7T or DDIN7T– PC_{61}BM (w/w) under illumination of AM.1.5, 100 mW cm^{-2} .

Table 2 Current density–voltage characteristics of the optimized SM BHJ devices

Active layer	V_{oc}/V	$J_{sc}/\text{mA cm}^{-2}$	FF	PCE (%)	$\mu_h/\text{cm}^2 \text{ V}^{-1} \text{ s}^{-1} \times 10^{-4}$
DCAO7T: $\text{PC}_{61}\text{BM}^a$	0.86	10.74	0.55	5.08	3.26
DERHD7T: $\text{PC}_{61}\text{BM}^b$	0.92	13.98	0.47	6.10	1.50
D2R(8 + 2)7T: $\text{PC}_{61}\text{BM}^c$	0.92	6.77	0.39	2.46	0.24
DTDMP7T: $\text{PC}_{61}\text{BM}^c$	0.90	7.54	0.60	4.05	0.47
DIN7T: PC_{61}BM with PDMS	0.80	8.56	0.72	4.93	1.73
DIN7T: PC_{61}BM	0.80	8.21	0.72	4.71	1.73
DDIN7T: PC_{61}BM	0.76	3.14	0.28	0.66	0.30

^a Data from ref. 35. ^b Data from ref. 30. ^c Data from ref. 36.

stacking in the film, which leads to the poor performance of the DDIN7T-based SM BHJ device.

For DIN7T, the optimal efficiency was obtained from the device with the active layer comprised of a blend of DIN7T and PC₆₁BM with a weight ratio of 1 : 1 and an optimized thickness of about 100 nm, using LiF/Al as the cathode. The optimal SM BHJ device showed a high PCE of 4.71%, with a J_{sc} of 8.21 mA cm⁻², a V_{oc} of 0.80 V and a notable FF of 0.72, which is the highest FF of solution-processed small molecule-based BHJ devices to date. Regarding the error range of the FF values, the FF values for over 100 devices of DIN7T-PC₆₁BM fall between 0.68 and 0.74, with an average of 0.72. Additionally, the value of 0.72 FF comes with the best overall PCE. The high FF is unique to DIN7T, even at different donor:PC₆₁BM ratios (Fig. S8 and Table S3†). The lower V_{oc} of DIN7T-based SM BHJs (0.80 V), compared with DCAO7T and DERHD7T, might be caused by two factors. First, the HOMO of the DIN7T molecule is higher than that of DCAO7T and DERHD7T; second, the better aggregation of DIN7T may also lead to an increase of the resulting HOMO levels.⁵⁰

Because of the outstanding performance of DIN7T, we further optimized the device mainly through improving the V_{oc} and J_{sc} . Using PC₇₁BM instead of PC₆₁BM as the acceptor led to a slight increase of J_{sc} to 8.51 mA cm⁻², while the FF decreased to 0.69, leading to a similar PCE of 4.70% with a V_{oc} of 0.80 V. Indene C₆₀ bisadduct (IC₆₀BA) was also chosen as the acceptor to improve the V_{oc} and the result is that V_{oc} increased to 1.0 V, while the J_{sc} and FF dropped sharply to 4.85 mA cm⁻² and 0.56, respectively, and thus a low PCE 2.75% was obtained. Different additives,^{51,52} such as 1,8-diiodooctane (DIO), 1-chloronaphthalene (CN) and polydimethylsiloxane (PDMS), were also tested as shown in Fig. S10–S13 and Table S2,† and it can be seen that there existed a balance between J_{sc} and FF. For the CN additive, it appears that addition suppresses aggregation too much, leading to a small domain (Fig. S13†) size, and thus a smaller FF. A similar case was observed for the addition of DIO (Fig. S13†). Finally, with the addition of 0.3 mg mL⁻¹ PDMS, the performance of the optimized devices was slightly improved to a PCE of 4.93%, with a V_{oc} of 0.80 V, a J_{sc} of 8.56 mA cm⁻² and a FF of 0.72. The improved efficiency is due to the slightly reduced domain size (probably closer to the ideal domain size for charge separation and transportation) in the active layer (Fig. S13†).

In order to further understand the device performance, the external quantum efficiency (EQE) of these two molecule-based devices was measured as shown in Fig. 6. From the curves, we can see that the DDIN7T- and DIN7T-based devices, similar to DERHD7T,³⁰ show much broader absorption regions than DCAO7T.³⁵ However, the EQE values of the DIN7T- and DDIN7T-based devices are all below 48% from 300 to 800 nm, much lower than DCAO7T and DERHD7T (about 60–70%). For DDIN7T-based SM BHJ devices, the lower EQE is mainly due to poor stacking and the low LUMO of the molecule. However, for DIN7T with good packing in the film, a suitable LUMO and good hole mobility, the EQE is still much lower.

The external quantum efficiency (EQE) can be represented by the product of each efficiency in the following fundamental

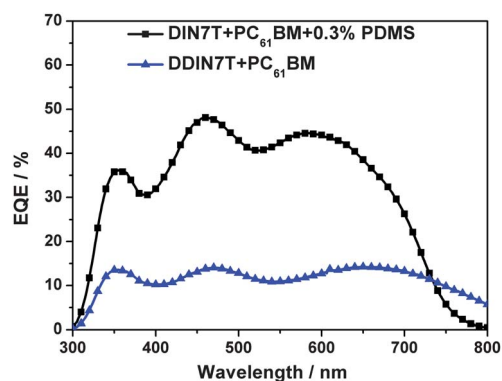


Fig. 6 EQE spectra of optimized SM BHJ devices of DIN7T:PC₆₁BM (1 : 1) and DDIN7T:PC₆₁BM (1 : 1).

processes: light absorption (η_A), exciton formation and migration (η_{ED}), exciton dissociation or charge separation (η_{CD}), charge transport (η_{CT}) and charge collection to the electrodes (η_{CC}).^{53–56} The lower EQE values of the DIN7T-based SM BHJ device might be caused by the process of η_{ED} . As shown in Fig. 7, the TEM and AFM images show that the DIN7T:PC₆₁BM active layer has an interpenetrating network with a large domain about 60 nm in size, much larger than that of the optimal domain size (10–20 nm) for η_{ED} .^{54,55} Thus, the large domain of the active layer leads to the relatively low photocurrent of the DIN7T-based SM BHJ device.

It can be seen that the fill factor of the DIN7T-based device is the highest in the series of oligothiophene donor-based SM BHJs in Table 1. The high FF of DIN7T-based SM BHJs could be due to many reasons,^{39,49} such as a low current leakage (Fig. S16†), the high hole mobility of DIN7T and a balanced hole (0.58×10^{-4} cm² V⁻¹ s⁻¹) and electron mobility (0.71×10^{-4} cm² V⁻¹ s⁻¹) in the blend film (Fig. S19 and S20†). Apart from the above test results, with respect to structure design, we can conclude that the high FF can be attributed to good molecular packing in the active layer (XRD shown in Fig. S7†). DIN7T has a good planar structure with two suitable planar end groups as π -stacking regulators which facilitate favorable π - π interactions as indicated in the XRD results, leading to enhanced bulk film order and more efficient intra- and intermolecular charge transport in the blend layer. Thus, the carrier transport process is dominant over charge carrier recombination and a high FF is displayed.²³

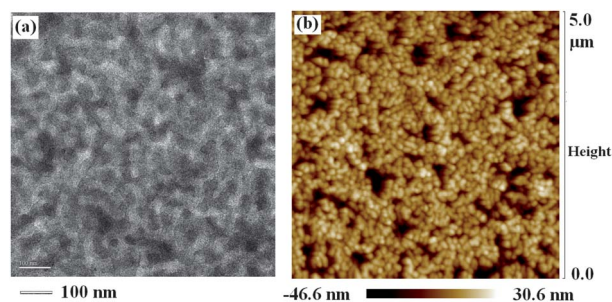


Fig. 7 TEM (a) and AFM (b) of the DIN7T:PC₆₁BM (1 : 1) active layer.

Conclusions

Three new end dye moieties acting as acceptor units were introduced to the oligothiophene based donor unit, forming three A–D–A type molecules DIN7T, DINCN7T and DDIN7T. The acceptor units not only have a huge effect on the band gaps and energy levels of these small molecules, but also have a great impact on the solubility of the molecules and the packing mode in the film. The poor packing in the solid state and the low LUMO level of DDIN7T lead to a relatively low PCE of 0.66%. Molecule DINCN7T lacked sufficient solubility to be processed into a SM BHJ device. In contrast, the DIN7T-based device has a high PCE of 4.93%, with the highest fill factor of 0.72 in SM BHJs, under illumination of AM.1.5, 100 mW cm⁻². These results indicate that the end group can serve two roles: (i) adjustment of solubility and the bandgap of the dyes, and (ii) directing self-assembly of molecules in the bulk film. Dedicated design and systematic investigation of the strategies that introduce a better planar structure to the end groups in A–D–A type dyes to regulate molecular assembly are highly needed to attain active layers with optimal and stable morphological and transport characteristics and finally improve the overall SM BHJ performance.

Acknowledgements

The authors gratefully acknowledge financial support from the NSFC (Grants 50933003, 50902073 and 50903044), MOST (Grants 2012CB933401 and 2011DFB50300) and NSF of Tianjin City (Grant 10ZCGHHZ00600). Professor Yongfang Li at the Institute of Chemistry, CAS, is also greatly appreciated for supplying the IC₆₀BA.

References

- 1 A. C. Arias, J. D. MacKenzie, I. McCulloch, J. Rivnay and A. Salleo, *Chem. Rev.*, 2010, **110**, 3.
- 2 Y. J. Cheng, S. H. Yang and C. S. Hsu, *Chem. Rev.*, 2009, **109**, 5868.
- 3 A. J. Heeger, *Chem. Soc. Rev.*, 2010, **39**, 2354.
- 4 G. Li, R. Zhu and Y. Yang, *Nat. Photonics*, 2012, **6**, 153.
- 5 D. Angmo, T. T. Larsen-Olsen, M. Jørgensen, R. R. Søndergaard and F. C. Krebs, *Adv. Energy Mater.*, 2012, DOI: 10.1002/aenm.201200520.
- 6 Z. He, C. Zhong, S. Su, M. Xu, H. Wu and Y. Cao, *Nat. Photonics*, 2012, **6**, 593.
- 7 Y. Li, *Acc. Chem. Res.*, 2012, **45**, 723.
- 8 X. Guo, C. Cui, M. Zhang, L. Huo, Y. Huang, J. Hou and Y. Li, *Energy Environ. Sci.*, 2012, **5**, 7943.
- 9 L. Huo, S. Zhang, X. Guo, F. Xu, Y. Li and J. Hou, *Angew. Chem., Int. Ed.*, 2011, **50**, 9697.
- 10 C. E. Small, S. Chen, J. Subbiah, C. M. Amb, S.-W. Tsang, T.-H. Lai, J. R. Reynolds and F. So, *Nat. Photonics*, 2012, **6**, 115.
- 11 S. Chen, C. E. Small, C. M. Amb, J. Subbiah, T.-h. Lai, S.-W. Tsang, J. R. Manders, J. R. Reynolds and F. So, *Adv. Energy Mater.*, 2012, **2**, 1333.
- 12 L. Dou, J. You, J. Yang, C.-C. Chen, Y. He, S. Murase, T. Moriarty, K. Emery, G. Li and Y. Yang, *Nat. Photonics*, 2012, **6**, 180.
- 13 Z. He, C. Zhong, X. Huang, W.-Y. Wong, H. Wu, L. Chen, S. Su and Y. Cao, *Adv. Mater.*, 2011, **23**, 4636.
- 14 T. Yang, M. Wang, C. Duan, X. Hu, L. Huang, J. Peng, F. Huang and X. Gong, *Energy Environ. Sci.*, 2012, **5**, 8208.
- 15 W. Chen, M. P. Nikiforov and S. B. Darling, *Energy Environ. Sci.*, 2012, **5**, 8045.
- 16 X. Yang, J. Loos, S. C. Veenstra, W. J. H. Verhees, M. M. Wienk, J. M. Kroon, M. A. J. Michels and R. A. J. Janssen, *Nano Lett.*, 2005, **5**, 579.
- 17 P. W. M. Blom, V. D. Mihailetchi, L. J. A. Koster and D. E. Markov, *Adv. Mater.*, 2007, **19**, 1551.
- 18 C. Risko, M. D. McGehee and J.-L. Bredas, *Chem. Sci.*, 2011, **2**, 1200.
- 19 M. T. Lloyd, J. E. Anthony and G. G. Malliaras, *Mater. Today*, 2007, **10**, 34.
- 20 B. Walker, C. Kim and T. Q. Nguyen, *Chem. Mater.*, 2011, **23**, 470.
- 21 R. Fitzner, E. Mena-Osteritz, A. Mishra, G. Schulz, E. Reinold, M. Weil, C. Körner, H. Ziehlke, C. Elschner, K. Leo, M. Riede, M. Pfeiffer, C. Urich and P. Bäuerle, *J. Am. Chem. Soc.*, 2012, **134**, 11064.
- 22 Y. Lin, Y. Li and X. Zhan, *Chem. Soc. Rev.*, 2012, **41**, 4245.
- 23 A. Mishra and P. Bäuerle, *Angew. Chem., Int. Ed.*, 2012, **51**, 2020.
- 24 H.-Y. Lin, W.-C. Huang, Y.-C. Chen, H.-H. Chou, C.-Y. Hsu, J. T. Lin and H.-W. Lin, *Chem. Commun.*, 2012, **48**, 8913.
- 25 D. Demeter, T. Rousseau, P. Leriche, T. Cauchy, R. Po and J. Roncali, *Adv. Funct. Mater.*, 2011, **21**, 4379.
- 26 Z. B. Henson, K. Mullen and G. C. Bazan, *Nat. Chem.*, 2012, **4**, 699.
- 27 W. L. Leong, G. C. Welch, L. G. Kaake, C. J. Takacs, Y. Sun, G. C. Bazan and A. J. Heeger, *Chem. Sci.*, 2012, **3**, 2103.
- 28 D. Credgington, F. C. Jamieson, B. Walker, T.-Q. Nguyen and J. R. Durrant, *Adv. Mater.*, 2012, **24**, 2135.
- 29 S. Loser, C. J. Bruns, H. Miyauchi, R. o. P. Ortiz, A. Facchetti, S. I. Stupp and T. J. Marks, *J. Am. Chem. Soc.*, 2011, **133**, 8142.
- 30 Z. Li, G. He, X. Wan, Y. Liu, J. Zhou, G. Long, Y. Zuo, M. Zhang and Y. Chen, *Adv. Energy Mater.*, 2012, **2**, 74.
- 31 Y. Sun, G. C. Welch, W. L. Leong, C. J. Takacs, G. C. Bazan and A. J. Heeger, *Nat. Mater.*, 2012, **11**, 44.
- 32 T. S. Van der Poll, J. A. Love, T.-Q. Nguyen and G. C. Bazan, *Adv. Mater.*, 2012, **24**, 3646.
- 33 J. Zhou, X. Wan, Y. Liu, Y. Zuo, Z. Li, G. He, G. Long, W. Ni, C. Li, X. Su and Y. Chen, *J. Am. Chem. Soc.*, 2012, **134**, 16345.
- 34 Y. Liu, X. Wan, B. Yin, J. Zhou, G. Long, S. Yin and Y. Chen, *J. Mater. Chem.*, 2010, **20**, 2464.
- 35 Y. Liu, X. Wan, F. Wang, J. Zhou, G. Long, J. Tian, J. You, Y. Yang and Y. Chen, *Adv. Energy Mater.*, 2011, **1**, 771.
- 36 G. He, Z. Li, X. Wan, Y. Liu, J. Zhou, G. Long, M. Zhang and Y. Chen, *J. Mater. Chem.*, 2012, **22**, 9173.
- 37 J. Zhou, X. Wan, Y. Liu, G. Long, F. Wang, Z. Li, Y. Zuo, C. Li and Y. Chen, *Chem. Mater.*, 2011, **23**, 4666.

- 38 Y. Liu, X. Wan, F. Wang, J. Zhou, G. Long, J. Tian and Y. Chen, *Adv. Mater.*, 2011, **23**, 5387.
- 39 O. P. Lee, A. T. Yiu, P. M. Beaujuge, C. H. Woo, T. W. Holcombe, J. E. Millstone, J. D. Douglas, M. S. Chen and J. M. J. Fréchet, *Adv. Mater.*, 2011, **23**, 5359.
- 40 H. Bürckstümmer, E. V. Tulyakova, M. Deppisch, M. R. Lenze, N. M. Kronenberg, M. Gsänger, M. Stolte, K. Meerholz and F. Würthner, *Angew. Chem.*, 2011, **123**, 11832.
- 41 Y. S. Liu, J. Y. Zhou, X. J. Wan and Y. S. Chen, *Tetrahedron*, 2009, **65**, 5209.
- 42 V. D. Mihailetschi, H. X. Xie, B. de Boer, L. J. A. Koster and P. W. M. Blom, *Adv. Funct. Mater.*, 2006, **16**, 699.
- 43 Y. Liang, D. Feng, Y. Wu, S.-T. Tsai, G. Li, C. Ray and L. Yu, *J. Am. Chem. Soc.*, 2009, **131**, 7792.
- 44 C. Kim, J. Liu, J. Lin, A. B. Tamayo, B. Walker, G. Wu and T.-Q. Nguyen, *Chem. Mater.*, 2012, **24**, 1699.
- 45 Y. Li, Y. Cao, J. Gao, D. Wang, G. Yu and A. J. Heeger, *Synth. Met.*, 1999, **99**, 243.
- 46 J. Cao, J. W. Kampf and M. D. Curtis, *Chem. Mater.*, 2002, **15**, 404.
- 47 Gaussian 09, Revision B.01, Gaussian, Inc., Wallingford CT, 2010. See ESI† for full citation.
- 48 W. Ma, C. Yang, X. Gong, K. Lee and A. J. Heeger, *Adv. Funct. Mater.*, 2005, **15**, 1617.
- 49 M.-S. Kim, B.-G. Kim and J. Kim, *ACS Appl. Mater. Interfaces*, 2009, **1**, 1264.
- 50 K. C. Deing, U. Mayerhoffer, F. Würthner and K. Meerholz, *Phys. Chem. Chem. Phys.*, 2012, **14**, 8328.
- 51 J. K. Park, C. Kim, B. Walker, T.-Q. Nguyen and J. H. Seo, *RSC Adv.*, 2012, **2**, 2232.
- 52 K. R. Graham, J. Mei, R. Stalder, J. W. Shim, H. Cheun, F. Steffy, F. So, B. Kippelen and J. R. Reynolds, *ACS Appl. Mater. Interfaces*, 2011, **3**, 1210.
- 53 K. Masuda, Y. Ikeda, M. Ogawa, H. Benten, H. Ohkita and S. Ito, *ACS Appl. Mater. Interfaces*, 2010, **2**, 236.
- 54 G. Li, V. Shrotriya, Y. Yao, J. Huang and Y. Yang, *J. Mater. Chem.*, 2007, **17**, 3126.
- 55 F. He and L. Yu, *J. Phys. Chem. Lett.*, 2011, **2**, 3102.
- 56 G. Chen, H. Sasabe, Z. Wang, X. Wang, Z. Hong, J. Kido and Y. Yang, *Phys. Chem. Chem. Phys.*, 2012, **14**, 14661.